URSI GASS 2021, Rome, Italy, 28 August - 4 September 2021

A Multiple Input Single Output Radar for Through-the-Wall Radar Imaging

Stefano Pisa[(1)], Renato Cicchetti[(1)], Emanuele Piuzzi[(1)], Orlandino Testa[(1)], and Paolo D'Atanasio[(2)]

(1) Department of Information Engineering, Electronics and Telecommunication, Sapienza University of Rome, Rome, Italy

(2) Italian National Agency for New Technologies, Energy and Sustainable Economic Development, Casaccia Research Centre, Rome, Italy

Abstract

A step frequency Radar for through-the-wall radar imaging applications, based on a vector network analyzer (VNA) and on a Multiple Input Single Output (MISO) architecture, is presented. The system was calibrated by removing the errors due to the connection cables, to the time delay introduced by the antennas and by the power amplifier. Using the Radar, the position of metallic targets both in the absence and in the presence of a wall was accurately identified. The data acquired by the Radar were processed using 4 algorithms present in the literature and a new FT-MUSIC algorithm developed by the Authors. All the considered algorithms were able to accurately reconstruct the position of the investigated targets both in the absence and in the presence of a wall.

1 Introduction

Through-the-Wall Radar Imaging (TWRI) Systems allow police, firefighters and defense forces to detect, identify and track individuals inside buildings [1]. Furthermore, they can also be used to follow the elderly into their home [2]. Typically, these systems use a time division (TDM) multi-input multiple-output (MIMO) antenna array and are based on frequency modulated continuous wave (FMCW) [3] - [4], ultra-wide band (UWB) [5] - [6] or step frequency (SF) [7] - [8] Radars. TWRI systems apply appropriate algorithms on the acquired signals to reconstruct an image of the investigated scenario. In [8] a MIMO system with 4 transmitting antennas and 4 receiving antennas was proposed (see Fig. 1). Four conventional algorithms (DAS, FT, MUSIC, DAS-MUSIC) and a new FT-MUSIC algorithm were used for the scenario reconstruction. In this paper, the same algorithms will be applied by using a faster system based on multiple input single output (MISO) Radar with 1 transmitting and 10 receiving antennas (see Fig. 2). The reconstruction algorithms will be compared considering a scenario constituted by a single bar and a metal panel placed behind a brick wall.

2 Experimental setup

A block scheme of the MISO step frequency Radar is shown in Fig. 3. The Agilent M5230A vector network analyzer is used to measure the transmission scattering

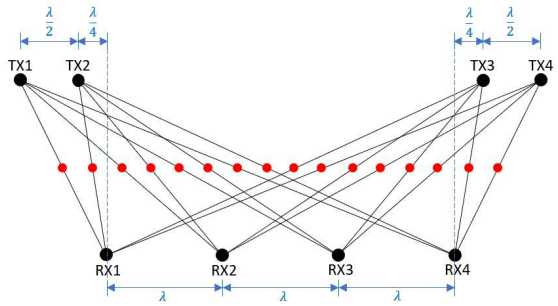

Figure 1. Antenna scheme of a MIMO Radar system.

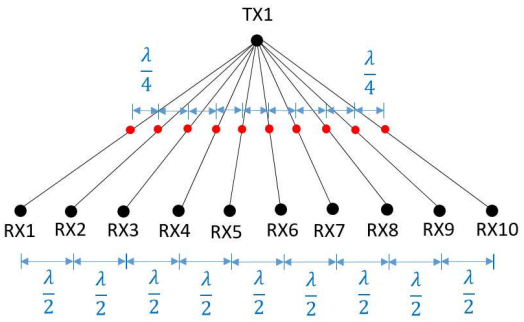

Figure 2. Antenna scheme of a MISO Radar system.

parameter (S_{21}) at $N_f = 500$ frequency points between 1 GHz and 3 GHz. Port 1 is connected to a transmitting Vivaldi antenna while port 2 is connected to a switch system able of selecting $N_a = 10$ receiving Vivaldi antennas [9]. The spatial positioning of the antennas is chosen as indicated in Fig. 2. In this way, a series of equidistant equivalent antennas separated by a quarter of the free-space wavelength at the central frequency of 2 GHz is realized. Following the spatial positioning indicated in Fig. 2, the antennas were housed in a wooden box (see Fig. 4). For measurements in the presence of the wall a 15 dB power amplifier (HP 8349A) (not shown in the figure) is added in the transmission channel. The antennas are selected via 3 electrically controlled switches. The first is the Analog Devices HMC344ALP3E which is driven by two control pins with negative signals. Two of the four RF outputs of the switch are sent to the input of two electromechanical switches (Pasternak PE71S6088). These switches are driven with TTL logic, and five of the six output channels are used to feed the 10 receiving antennas (see schematic of the MISO radar shown in Fig. 3).

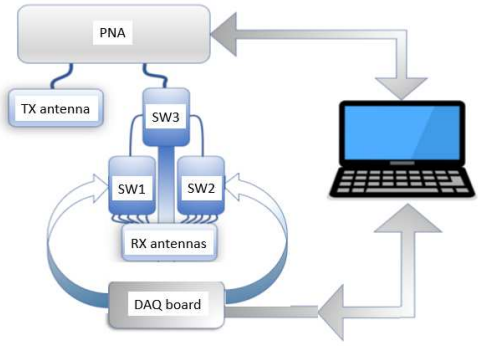

Figure 3. Diagram of the realized MISO Radar.

Figure 4. Picture of the MISO Radar antenna system.

All driving signals are provided by the National Instruments DAQ board NI USB-6251 which is controlled by a program written in the LabVIEW environment. In turn, the scattering parameters measured by the VNA are acquired through a GPIB interface controlled by the LabVIEW program. The complex scattering parameters are saved in a ($N_a \times N_f$) matrix. Finally, the imaging algorithms implemented in Matlab are applied to the collected data.
Before taking the measurements, the system is calibrated between the port of the transmitting antenna and the port of one of the receiving antennas. A measurement error not removed by the calibration is the one due to the propagation delay of the signal introduced by the Vivaldi antennas. This error was estimated, and corrected, through a set of measurements in which two antennas, connected to the two PNA ports, are placed opposite to each other at a certain distance. By measuring the time domain impulse response, the time delay due to the physical distance between the two antennas plus the one introduced by the antennas has been evaluated. This measurement is repeated for different distances and finally, through a linear regression, the value of the intersection point between the fit line and the ordinate axis is found. This value corresponds to the temporal position of the peak when the distance between the two antennas is zero and therefore coincides with the delay of the antenna system.

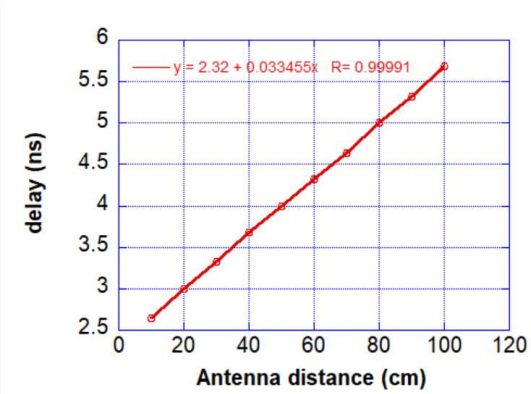

Figure 5. Delay measured as a function of the distance between the antennas.

In particular, 10 measurements were made by initially positioning the antennas at a relative distance of 1 m and bringing them closer by 10 cm at a time. The result of the measurements is shown in Fig. 5. The measurements were interpolated using the linear equation: $y = 0.0335x + 2.32$. Therefore, the delay associated with the antenna system is about 2.32 ns. When using the HP8349A amplifier in the transmission channel, this produces a further delay which has been evaluated by the phase slope of the S_{21} scattering parameter of the amplifier obtaining 5 ns.

4 Experimental Results

The measurements were carried out in a room of the Enea-Casaccia research center.

4.1 Measurements in the absence of the wall

The first scenario investigated consisted of a metal pipe with a 10 cm diameter and 100 cm high, placed 1.4 meters away from the plane of the antennas (see Fig. 6). The wooden support with the antennas was positioned 40 cm from the ground, therefore the equivalent antenna array is 66.5 cm high. The previously described procedure has been used to evaluate the scattering parameters at 500 frequency points between 1 and 3 GHz (frequency band B = 2 GHz, frequency step δf = 4 MHz).

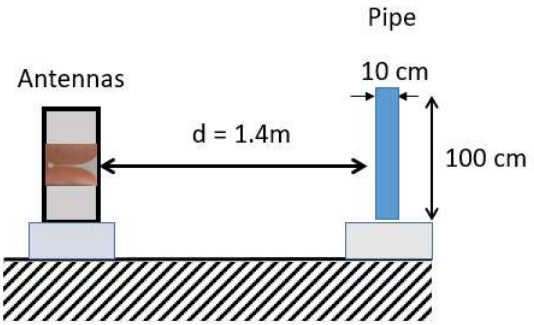

Figure 6. Schematic of the first investigated scenario.

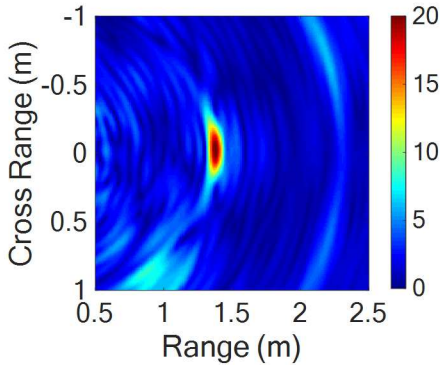

Figure 7. Image reconstruction with DAS.

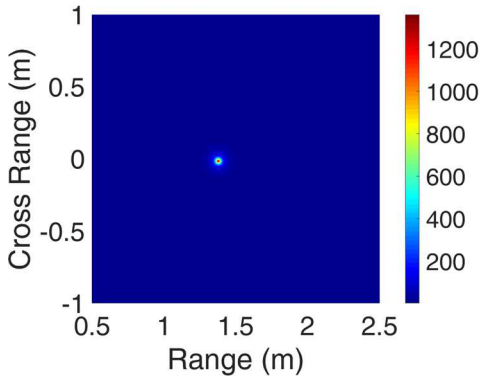

Figure 8. Image reconstruction with FT-MUSIC.

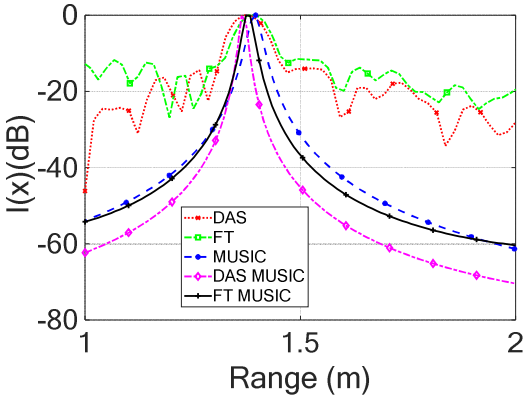

Figure 9 Range cutting of the acquired image: comparison between reconstruction techniques.

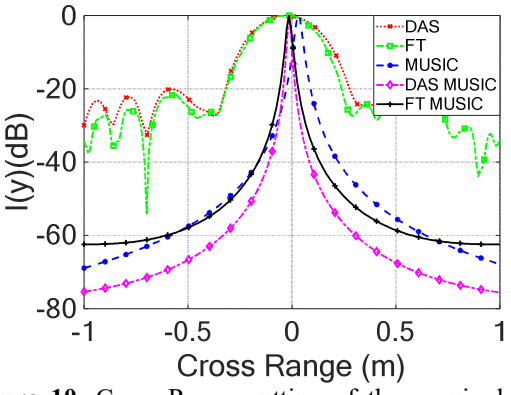

Figure 10. Cross Range cutting of the acquired image: comparison between reconstruction techniques.

For the considered scenario the Radar theoretical resolution in range is $\delta r = c / 2B = 7.5$ cm, the angular resolution is $\delta\theta = 2 / (N_a - 1) = 0.22$ rad (12.7°), and the unambiguous range is $R_{max} = c / 2\delta f = 37.5$ m.

Fig. 7 and Fig. 8 show the results of scenario reconstructions performed using the DAS and FT-MUSIC algorithms, respectively. Fig. 9 and Fig. 10 report a comparison between the five considered techniques. The figures show cuts along the range (Fig. 9) and cross-range (Fig. 10) directions performed on the image reconstructions. In particular, the normalized intensity function in dB is reported with respect to the position. From the figures it results a half power beam width (HPBW) for both DAS and FT equal to 8 cm in range (Fig. 7) and 27 cm in cross-range (Fig. 8) very close to 7.5 and 30 cm theoretical resolutions obtainable from the array. The HPBW in range is 2.5 cm for MUSIC and FT-MUSIC and 2 cm for DAS-MUSIC. Cross range resolution is 2 cm for MUSIC, 1.5 cm for FT-MUSIC and 1 cm for DAS-MUSIC. These results highlight the better performance of the MUSIC, DAS-MUSIC and FT-MUSIC algorithms compared to DAS and FT in particular along the cross-range direction.

4.2 Measurements in the presence of the wall

In this experiment, the presence of a 25 cm thick tuff wall placed 2.25 meters from the plane of the antennas and of a metal panel placed at 50 cm from the wall was considered (see Fig. 11). To reduce the effect of the environment, the scattering parameters used in the reconstruction algorithms were evaluated through the mathematical difference between those measured in the presence and absence of the obstacle, thus carrying out a sort of calibration. To take into account the refraction effect caused by the wall, the hypothesis of an almost normal incidence on the wall of the field generated by the Radar was made. In this case, the wall effect can be taken into account by simply adding an additional delay term given by:

$$\tau_w = \frac{2d}{c}\left(\sqrt{\varepsilon_r'} - 1\right)$$

where d is the wall thickness and ε_r' is the real relative dielectric permittivity. For the relative permittivity of the tuff wall the value of 3.5 has been used as suggested in [10] Fig. 12 and Fig. 13 show the results of the simulations performed using the five considered techniques. The figures show cuts along the range (Fig. 12) and cross-range (Fig. 13) directions performed on the image reconstructions based on the techniques considered. In particular, the normalized intensity function in dB is reported with respect to the position.

As can be seen from Fig. 12, thanks to the τ_w correction all the techniques correctly reconstruct the distance of the panel. The best performances of super-resolution

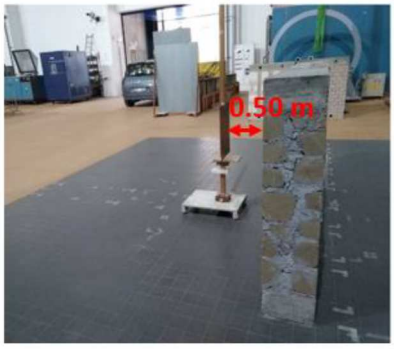

Figure 11. Scheme of the second investigated scenario.

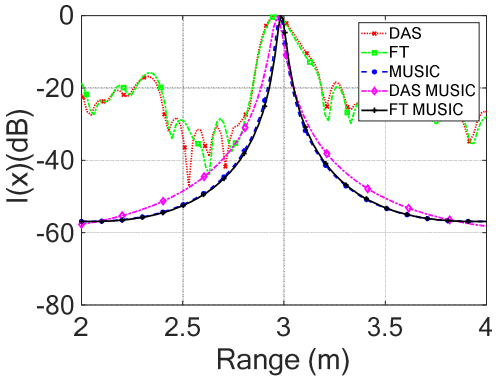

Figure 12. Range cutting of the acquired image: Comparison between various reconstruction techniques.

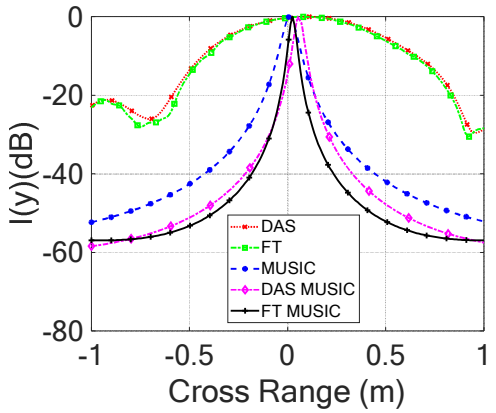

Figure 13. Cross Range cutting of the acquired image: Comparison between various reconstruction techniques.

techniques are highlighted in cross-range reconstructions where, due to the increase in distance compared to the previous case, the HPBW of the DAS and FT techniques is even greater.

5 Conclusions

In this work, a MISO radar has been used to acquire images of scatterers in scenarios with and without walls. The system has been calibrated by removing the errors connected to the connection cables, to the delay introduced by the antennas and the one introduced by the amplifier. For scenarios in the presence of a wall, the additional delay introduced by the wall itself was considered. The acquired data were processed using 5 different algorithms. All the algorithms were able to accurately reconstruct the position of the investigated target both in the absence and in the presence of the wall. With the proposed MISO Radar system acquisition times of the order of 10 s have been obtained that are 50% lower than those of the MIMO system presented in [8].

6 References

1. M.G. Amin, “Through the wall radar imaging”, CRC Press, 2011.
2. G. Wang, C. Gu, T. Inoue, C. Li, “A hybrid FMCW-interferometry radar for indoor precise positioning and versatile life activity monitoring,” *IEEE Trans. on Microwave Theory and Techniques*, **62**, 11, pp. 2812-2822, 2014.
3. G. L. Charvat, L. C. Kempel, E. J. Rothwell, C. M. Coleman, and E. L. Mokole, “A through-dielectric radar imaging system,” *IEEE Transactions on Antennas and Propagation*, **58**, 8, pp. 2594-2603, Aug. 2010.
4. G. Sacco, E. Piuzzi, E. Pittella, S. Pisa, “An FMCW Radar for localization and vital signs measurement for different chest orientations,” *Sensors*, **20**, 2, pp. 1-14, 2020.
5. M. A. Ressler, L. H. Nguyen, F. J. Koenig, G. Smith, “Synchronous impulse reconstruction (SIRE) radar sensor for autonomous navigation,” *US Army Research Laboratory*, 2006.
6. S. Pisa, P. Bernardi, M. Cavagnaro, E. Pittella, and E. Piuzzi, “A circuit model of an ultra-wideband impulse radar system for breath-activity monitoring,” *Int. J. Numer. Model.*, **25**, 1, pp. 46-63, January-February 2012.
7. X. P. Masbernat, M. G. Amin, F. Ahmad, C. Ioana, “An MIMO-MTI Approach for Through-the-Wall Radar Imaging Applications,” Proc. *5th Int. Waveform Diversity and Design Conf.*, Canada, 2010, pp. 188-192.
8. R. Cicchetti, S. Pisa, E. Piuzzi, E. Pittella, P. D’Atanasio, and O. Testa, “Numerical and experimental comparison among a new hybrid FT-Music technique and existing algorithms for through-the-wall radar imaging,” Accepted for publication: *IEEE Trans. on Microwave Theory and Techniques*.
9. R. Cicchetti, E. Miozzi, and O. Testa, “Wideband and UWB antennas for wireless applications: A comprehensive review,” *Int. J. Antennas Propag.*, **2017**, Art. no. 2390808.
10. R. Agliata; L. Mollo; and R. Greco, “Use of TDR to compare rising damp in three tuff walls made with different mortars,” *Journal of Materials in Civil Engineering*, pp. 1-7, November 2016.